

# Testing the double-logarithm asymptotic gluon density in ultraperipheral heavy ion collisions at the Large Hadron Collider

D. A. Fagundes<sup>✉\*</sup>

*Department of Exact Sciences and Education, CEE. Federal University of Santa Catarina (UFSC) - Blumenau Campus, 89065-300, Blumenau, SC, Brazil*

M.V.T. Machado<sup>✉†</sup>

*High Energy Physics Phenomenology Group, GFPPE. Institute of Physics, Federal University of Rio Grande do Sul (UFRGS) Postal Code 15051, CEP 91501-970, Porto Alegre, RS, Brazil*

In this paper, we analyze the application of an analytical gluon distribution based on double-asymptotic scaling to the photoproduction of vector mesons in coherent  $pp$ ,  $pA$ , and  $AA$  collisions at LHC energies, using the color dipole formalism. Predictions for the rapidity distribution are presented for  $\rho^0$ ,  $J/\psi$ ,  $\psi(2S)$ , and  $\Upsilon(1S)$  mesons photoproduction. An analysis of the uncertainties associated with different implementations of the dipole–proton amplitude is performed. The vector meson photoproduction accompanied by electromagnetic dissociation is also analyzed.

## I. INTRODUCTION

The exclusive production of vector mesons plays a crucial role both experimentally and theoretically, enabling accurate studies on applications of perturbative quantum chromodynamics (QCD) and parton saturation physics. Light vector mesons, on one hand, have no hard (of transverse momentum above 1 GeV) perturbative scale associated with the process in the photoproduction limit, with the incoming photon’s virtuality  $Q^2 = 0$ , thus probing the non-perturbative regime of QCD. In the electroproduction case, where  $Q^2$  is sufficiently large, a perturbative approach is justified. On the other hand, quarkonium production involves an intrinsic hard scale characterized by the heavy quark masses, even at  $Q^2 = 0$ , and weak coupling methods can be successfully applied. It is known ultratransverse momentum below 1 GeV that the transition between the perturbative QCD treatment and the soft regime can be handled by the parton saturation framework [1–11] within the QCD color dipole formalism [12–15]. There, the saturation scale,  $Q_s$ , sets the limit on the parton phase-space density that can be reached in the hadron’s wavefunction. Hence, it can be viewed as the typical underlying scale in low enough Bjorken- $x$  dynamics for light meson photoproduction (with  $x$  a fraction of the hadron’s longitudinal momentum carried by a parton) and also plays a key role in quarkonium production (see recent applications in Refs. [16–35] and references therein). The photon–proton ( $\gamma p$ ) or photon–nucleus ( $\gamma A$ ) scattering in such an approach is characterized by the QCD color dipole amplitude, which represents the interaction of the Fock states of the incoming virtual photon, i.e., color singlet dipoles at leading order, with the target at rest. The quark–anti-quark ( $q\bar{q}$ ) fluctuations and the transition from the dipole to meson are described by the photon and vector meson wavefunctions, respectively.

Given the shutdown of the Hadron-Electron Ring Accelerator (HERA) experiment, low- $x$  studies of exclusive processes are now being actively pursued in relativistic heavy-ion collisions and at the Large Hadron Collider (LHC). In ultraperipheral heavy-ion collisions (UPCs) and coherent proton–proton ( $pp$ ) reactions, the production process can be theoretically factorized into the high photon flux from the hadron or nucleus projectile and the photon–target production cross-section [36–40]. Investigations into  $\gamma p$  or  $\gamma A$  interactions at these colliders provide valuable information about the underlying QCD dynamics. A key piece of information that can be extracted from the available meson production data is the gluon distribution function,  $xg(x, \mu^2)$ , where  $\mu$  is the characteristic hard scale.

Recently, in Ref. [41], the gluon parton distribution function (PDF) was evaluated by us based on double-asymptotic scaling (DAS) for gluon density [42, 43] within the color dipole approach. The model has the advantage of replacing the numerical LO DGLAP evolution at large virtualities with analytical calculations from pQCD in the DAS approximation. The evolution presents similar results compared to other studies [44, 45] using numerical DGLAP evolution. Reference [41] contributes to a considerably easier modeling of the dipole cross-section and requires only a little computational power to predict inclusive and exclusive deep inelastic scattering (DIS) observables. Regarding vector meson production, the calculations of  $J/\psi$  and  $\rho$  mesons photoproduction cross-sections describe both the HERA data

---

\*E-mail me at: daniel.fagundes@ufsc.br

†E-mail me at: magno.machado@ufrgs.br

and the measurements of vector meson photoproduction in  $pp$  collisions at the LHC. Moreover, as shown in Ref. [41], the extracted analytical gluon density is quite suitable for the high-precision HERA data and for studying small- $x$  physics at future colliders such as the Electron Ion Collider (EIC) and the Large Hadron Electron Collider (LHeC).

The main focus of the current paper is to investigate the robustness of the phenomenological model for the color dipole amplitude based on DAS approximation as applied to UPCs and  $pp$  collisions at the LHC energies. We analyze the theoretical uncertainties on the predictions of exclusive production of vector mesons in  $pp$ ,  $p\text{Pb}$ ,  $\text{PbPb}$  collisions at the LHC, providing predictions for the rapidity distribution,  $y$ . This paper is organized as follows. In Section II, we present the color dipole scattering amplitude that incorporates QCD evolution through the DAS approximation. The parameters of the model were determined from small- $x$  high-precision DIS electron-proton ( $ep$ ) data; the model correctly describes the structure functions and exclusive vector meson production. In Section III, we apply the formalism in order to compute the production of vector mesons in UPCs, focusing on the LHC energy regime. In the last Section, the results obtained are discussed.

## II. THEORETICAL FRAMEWORK AND PHENOMENOLOGICAL MODELS

Let us start by defining the ansatz for the gluon density based on the DAS approximation investigated in Ref. [41]. Given the sufficiently soft behavior at the input scale,  $Q_0$ , one obtains the double-asymptotic scaling for the gluon density as follows [42, 43]:

$$xg_{\text{DAS}}(x, \mu^2) = \frac{A_g}{\sqrt{4\pi\gamma\sigma}} \exp\left(2\gamma\sigma - \delta\frac{\sigma}{\rho}\right), \quad (1)$$

$$\gamma = \sqrt{12/\beta_0}, \quad \delta = \left(11 + \frac{2N_f}{27}\right) / \beta_0, \quad (2)$$

where  $A_g$  denotes the overall normalization of the distribution and  $\beta_0 = 11 - \frac{2}{3}N_f$  (with  $N_f$  the number of active flavors) denotes the first term of the QCD beta-function series. The geometric mean  $\sigma$  and the ratio  $\rho$  define the double-scaling variables:

$$\sigma \equiv \sqrt{\ln\left(\frac{x_0}{x}\right) \ln\left(\frac{t}{t_0}\right)}, \quad \rho \equiv \sqrt{\ln\left(\frac{x_0}{x}\right) / \ln\left(\frac{t}{t_0}\right)}, \quad (3)$$

$$t/t_0 \equiv \ln(\mu^2/\Lambda_{\text{QCD}}^2) / \ln(Q_0^2/\Lambda_{\text{QCD}}^2), \quad (4)$$

where the parameters  $x_0 \simeq 10^{-1}$  and  $Q_0^2 \simeq 1 \text{ GeV}^2$  define the boundaries of the asymptotic domain, and  $\Lambda_{\text{QCD}}$  represents the QCD scale parameter [46]. Accordingly, the  $xg$  exhibits asymptotic scaling in both  $\sigma$  and  $\rho$  in the double limit of large  $\sigma$  ( $\sigma \rightarrow \infty$ ) at fixed but reasonably large  $\rho$  and large  $\rho$  ( $\rho \rightarrow \infty$ ) at fixed  $\sigma$ . The original DAS ansatz provides an exceptionally good description of DIS data, as demonstrated by the last three rows of Table I, which follows from our previous study [41].

In Ref. [41], the form in Equation (1) was modified, enabling the smooth transition from large ( $x \rightarrow 1$ ) to lower ( $x \rightarrow 0$ ) values of  $x$  in  $xg$ . Namely, in the modified DAS model, the following form was considered:

$$xg_{\text{FM}}(x, \mu^2) = xg(x, \mu_0^2) \exp\left(2\gamma\sigma' - \delta\frac{\sigma}{\rho'}\right), \quad (5)$$

$$\text{with } xg(x, \mu_0^2) = A_g x^{-\lambda_g} (1-x)^{C_g},$$

where  $xg(x, \mu_0^2)$ , with  $\mu_0$  the initial evolution scale, represents the soft gluon ansatz (with  $C_g = 6.0$ ,  $\lambda_g$  is the low- $x$  effective power), and the rescaled geometric mean and ratio are now given by  $\sigma' = \sigma\ell(x)$  and  $\rho' = \rho\ell(x)$ , respectively. The function  $\ell(x) = \sqrt{\mathcal{N}(1-x)^5}$ , in which  $\mathcal{N}$  represents a new free parameter of the model, controls the normalization of  $xg(x, \mu^2)$  with the evolution of  $\mu^2$ . Such a factor corrects both the overall gluon normalization and the transition to larger  $x$  in the asymptotic term  $e^{2\gamma\sigma}$  within the original expression.

TABLE I: Fit parameters of the DAS model in Equation (1) for  $Q^2 \in (1.5, 50)$  GeV<sup>2</sup> and  $x \leq 0.001$ , including charm and bottom quarks. All fit parameters are provided at a 70% confidence level, with the masses  $m_{lq} = 0.03$  GeV of light quarks,  $m_c = 1.3$  GeV of  $c$  quark, and  $m_b = 4.2$  GeV of  $b$  quark, while  $\mu_0$  is defined in Equation (5) and  $\sigma_0$  is defined in Equation (8).

Model	$\sigma_0$ [mb]	$A_g$	$x_0$	$\mu_0^2$ [GeV <sup>2</sup> ]	$\chi^2/\text{dof}$	p-Value
BGK	$(172.4 \pm 2.9) \times 10^5$	$1.624 \pm 0.0041$	1.0 (fixed)	1.1 (fixed)	$1485.02/288 = 5.16$	0
	$295 \pm 29$	$2.834 \pm 0.017$	0.1 (fixed)	1.1 (fixed)	$306.848/288 = 1.07$	0.213
	$194 \pm 17$	$3.047 \pm 0.074$	$0.0805 \pm 0.0078$	1.1 (fixed)	$303.262/287 = 1.06$	0.244
	$114 \pm 11$	$3.80 \pm 0.32$	$0.0496 \pm 0.0095$	$1.29 \pm 0.13$	$290.576/286 = 1.02$	0.414

Given the DAS approximation, the QCD color dipole amplitude can be obtained. In the target rest frame, the DIS  $ep$  process,  $\gamma^* p \rightarrow X$ , where  $\gamma^*$  denotes the virtual photon and  $X$  denotes all produced hadrons, is viewed as the interaction of a color singlet  $q\bar{q}$  pair with fixed transverse size  $\vec{r}$  scattering off the target through gluon exchanges (gluon ladder diagrams). For instance, in the impact-parameter saturation model (IPSAT) [45, 47, 48], which describes the multiple interactions of a QCD dipole probe with a dense target, the  $b$ -dependent dipole amplitude is given as

$$\frac{d\sigma_{q\bar{q}}}{d^2\vec{b}} = 2 \left[ 1 - \exp \left( -\frac{\pi^2}{2N_c} r^2 \alpha_S(\mu^2) x g(x, \mu^2) T(b) \right) \right], \quad (6)$$

where  $T(b)$  represents the thickness function of a proton,  $N_c$  denotes the number of colors,  $\alpha_S$  represents the strong interaction coupling, the scale is set as  $\mu^2 = C/r^2 + \mu_0^2$ , and  $x$  denotes the modified Bjorken variable,  $x = x_{\text{Bj}}(1 + 4m_q^2/Q^2)$ , with  $x_{\text{Bj}}$  being a fraction of proton carried by the struck quark and  $m_q$  being the effective quark mass [49, 50]. Such a modification consistently describes the transition from high enough  $Q^2$  toward the limit  $Q^2 \rightarrow 0$ . Thus, the corresponding dipole cross-section is obtained as  $\hat{\sigma}(x, \vec{r}) = \int d^2\vec{b} d\sigma_{q\bar{q}}/d^2\vec{b}$ .

Generally, a Gaussian model is assumed for  $T(b)$ , given the exponential fall-off in the  $|t|$ -dependence of quarkonia production, with  $t$  denoting the momentum transfer. In such a case, the normalized-to-unity thickness,  $T_G(b)$ , is given as

$$T_G(b) = \frac{1}{2\pi B_G} \exp \left( -\frac{b^2}{2B_G} \right), \quad (7)$$

where the parameter  $B_G \simeq 4$  GeV<sup>2</sup> is related to the average squared transverse radius of the nucleon,  $\langle b^2 \rangle = 2B_G$  [45, 47, 48].

On the other hand, in the BGK approach [51–53], the color dipole cross-section reads

$$\hat{\sigma}(x, \vec{r}) = \sigma_0 \left[ 1 - \exp \left( -\frac{\pi^2 r^2 \alpha_S(\mu^2) x g(x, \mu^2)/N_c}{\sigma_0} \right) \right], \quad (8)$$

where  $\sigma_0$  is now a new parameter of this model. The unintegrated gluon distribution (UGD)  $\mathcal{F}(x, k)$ —the distribution probability of a gluon with a transverse momentum  $k$  and longitudinal momentum fraction  $x$  to be found in the nucleons—can be obtained from the dipole cross-section (8) as [54, 55]

$$\mathcal{F}(x, k) = k^4 \frac{\sigma_0}{\alpha_S(\mu_0^2)} \frac{N_c}{8\pi^2} \int_0^\infty r dr J_0(kr) \left[ 1 - \frac{\alpha_S(\mu_0^2)}{\alpha_S(r)} \frac{\hat{\sigma}(x, r)}{\sigma_0} \right], \quad (9)$$

where  $J_0(\cdot)$  represents the zeroth-order Bessel function of the first kind.

For the DIS-inclusive process, the cross-section for the interaction of a virtual photon with virtuality  $Q^2$  with a given polarization off a proton target is expressed as [56]:

$$\sigma_{T,L}^{\gamma^* p}(x, Q^2) = \sum_f \int d^2\vec{r} \int dz \left| \psi_{T,L}^f(Q, r, z) \right|^2 \hat{\sigma}(x, \vec{r}), \quad (10)$$

where  $\psi_{T,L}^f(Q, r, z)$  denotes the corresponding photon wave function in the mixed representation for a photon with transverse,  $T$ , or longitudinal,  $L$ , polarization, respectively. The quark (antiquark) carries a longitudinal momentum fraction  $z$  ( $1 - z$ ) of the incoming photon. The summation above refers to the quark flavor,  $f$ . The squared photon

wave functions, summed over quark helicities for a given photon polarization and quark flavor,  $f$ , are expressed by [56]:

$$\left| \psi_T^f(Q, r, z) \right|^2 = \frac{2N_c}{\pi} \alpha_{\text{em}} e_f^2 \left\{ [z^2 + (1-z)^2] \epsilon^2 K_1^2(\epsilon r) + m_f^2 K_0^2(\epsilon r) \right\}, \quad (11)$$

$$\left| \psi_L^f(Q, r, z) \right|^2 = \frac{8N_c}{\pi} \alpha_{\text{em}} e_f^2 Q^2 z^2 (1-z)^2 K_0^2(\epsilon r), \quad (12)$$

where  $\alpha_{\text{em}}$  is the electromagnetic coupling,  $e_f$  and  $m_f$  denote the  $f$ -flavor quark's charge and mass, respectively,  $K_\nu(\cdot)$  denotes the modified Bessel functions of the second kind of the order  $\nu = 0$  and 1, and  $\epsilon = \sqrt{z(1-z)Q^2 + m_f^2}$ .

The exclusive processes can also be described within the very same QCD color dipole picture. For example, the differential cross-section for exclusive vector meson ( $V$ ) production,  $\gamma^* p \rightarrow Vp$ , is given by [57]:

$$\frac{d\sigma^{\gamma p \rightarrow Vp}}{dt} = \frac{1}{16\pi} |\mathcal{A}^{\gamma p \rightarrow Vp}|^2 (1 + \beta^2) R_g^2, \quad (13)$$

where  $\mathcal{A}^{\gamma p \rightarrow Vp}$  represents the color dipole scattering amplitude defined below in this Section, and the real-to-imaginary ratio of the scattering amplitude,  $\beta$ , and the skewness factor,  $R_g$ , are computed as follows:

$$\beta = \tan\left(\frac{\pi\lambda_{\text{eff}}}{2}\right), \quad \text{with} \quad \lambda_{\text{eff}} \equiv \frac{\partial \ln\left(\mathcal{A}_T^{\gamma p \rightarrow Vp}\right)}{\partial \ln(1/x)}, \quad (14)$$

$$R_g(\lambda_{\text{eff}}) = \frac{2^{2\lambda_{\text{eff}}+3} \Gamma(\lambda_{\text{eff}} + 5/2)}{\sqrt{\pi} \Gamma(\lambda_{\text{eff}} + 4)}, \quad (15)$$

where  $\Gamma(\cdot)$  is the gamma function.

The factor  $R_g$  incorporates the off-diagonal effect, coming from the fact that the gluons attached to the  $q\bar{q}$  can carry different light-front fractions  $x, x'$  of the nucleon. The factor given in Equation (15) was obtained at the NLO level, in the limit that  $x' \ll x \ll 1$  and at small  $t$ , assuming that the diagonal gluon density of the proton follows a power-law form [58] (see the discussion in Ref. [59]). This phenomenological approach has been considered extensively in the literature. Anyway, for relatively small dipoles (dominant for heavy-meson production), the dipole cross-section or amplitude is proportional to the diagonal gluon distribution, which to be corrected by the Shuvaev formula in the off-diagonal case. In the past, the skewness factor has been extracted from the data by comparing the amplitudes for deeply virtual Compton scattering (DVCS) and the DIS amplitude (see, e.g., Refs. [60–62]). The parametrization in Equation (15) is satisfactory enough at describing it.

The elastic scattering amplitude for the process  $\gamma p \rightarrow Vp$  is a function of  $x$  and of the momentum transfer  $\vec{\Delta}$  (with  $|t| = \vec{\Delta}^2$ ), written as a Fourier transform of the photon and vector meson wavefunctions convoluted with the color dipole scattering amplitude transverse ( $T$ ) or longitudinal ( $L$ ) polarization contributions [57]:

$$\mathcal{A}_{T,L}^{\gamma p \rightarrow Vp} = i \int d^2\vec{r} \int_0^1 \frac{dz}{4\pi} \int d^2\vec{b} (\Psi_V^* \Psi_\gamma)_{T,L} e^{-i[\vec{b} - (1-z)\vec{r}] \cdot \vec{\Delta}} \frac{d\sigma_{q\bar{q}}}{d^2\vec{b}}, \quad (16)$$

$$= i\pi \int_0^\infty r dr \int_0^1 dz \int_0^\infty b db (\Psi_V^* \Psi_\gamma)_T J_0(b\Delta) J_0([1-z]r\Delta) \frac{d\sigma_{q\bar{q}}}{d^2\vec{b}}. \quad (17)$$

The overlap function,  $\Psi_V^* \Psi_\gamma$ , between the photon and the vector-meson wave functions is commonly known. Here, we are interested in vector-meson photoproduction, and the corresponding overlap involves only the transverse polarization contribution. In this case, the wave function at  $Q^2 = 0$  simplifies to

$$(\Psi_V^* \Psi_\gamma)_T = \hat{e}_f \sqrt{4\pi\alpha_{\text{em}}} \frac{N_c}{\pi z(1-z)} \left\{ m_f^2 K_0(\epsilon r) \phi_T(r, z) - [z^2 + (1-z)^2] \epsilon K_1(\epsilon r) \partial_r \phi_T(r, z) \right\}, \quad (18)$$

where  $\hat{e}_f$  denotes the effective charge,  $\phi_T(r, z)$  is the scalar part of the meson wave function in the case of transverse polarization as defined just next, and  $\partial_a \equiv \partial/\partial a$ .

In this study, the boosted Gaussian wave function [57] is considered, where the scalar part of the transversely or longitudinally polarized meson wave function  $\phi_{T,L}$  is expressed as follows. For the ground state vector meson (1S) and its first excited state (2S), one has [63–66]:

TABLE II: Parameters of the boosted Gaussian wave function for the vector mesons analyzed. See text for details.

Meson	$M_V$ [GeV]	$m_f$ [GeV]	$\mathcal{N}_T$	$\mathcal{N}_L$	$\mathcal{R}$ [GeV $^{-1}$ ]	$\alpha_{2S}$	$\Gamma_{V \rightarrow e^+e^-}^{\text{exp}}$ [keV]	$\Gamma_{V \rightarrow e^+e^-}^{\text{calc}}$ [keV]	Ref.
$\rho$	0.7753	0.030	0.9942	0.8928	3.6388	–	$7.04 \pm 0.06$	7.04	[41]
$J/\psi$	3.097	1.3	0.5974	0.5940	1.5181	–	$5.53 \pm 0.11$	5.53	[41]
$\psi(2S)$	3.686	1.3	0.70	0.69	1.93	-0.61	$2.33 \pm 0.08$	2.35	[66]
$\Upsilon$	9.460	4.2	0.6866	0.6696	0.3354	–	$1.29 \pm 0.07$	1.29	This study

$$\phi_{T,L}^{(1s)}(r, z) = \mathcal{N}_{T,L} z(1-z) \exp\left(-\frac{m_f^2 \mathcal{R}^2}{8z(1-z)} - \frac{2z(1-z)r^2}{\mathcal{R}^2} + \frac{m_f^2 \mathcal{R}^2}{2}\right), \quad (19)$$

$$\begin{aligned} \phi_{T,L}^{(2S)}(r, z) &= \mathcal{N}'_{T,L} z(1-z) \exp\left(-\frac{m_f^2 \mathcal{R}'^2}{8z(1-z)} - \frac{2z(1-z)r^2}{\mathcal{R}'^2} + \frac{m_f^2 \mathcal{R}'^2}{2}\right) \\ &\times \left[1 + \alpha_V \left(2 + \frac{m_f^2 \mathcal{R}'^2}{4z(1-z)} - \frac{4z(1-z)r^2}{\mathcal{R}'^2} - m_f^2 \mathcal{R}'^2\right)\right], \end{aligned} \quad (20)$$

where the parameter  $\alpha_V$  controls the position of the node of the radial wave function of the excited state. The corresponding parameters  $\mathcal{N}_{T,L}$  ( $\mathcal{N}'_{T,L}$ ) and  $\mathcal{R}$  ( $\mathcal{R}'$ ) are properly obtained from both wave function normalization and the constraint from the electronic decay width,  $\Gamma_{V \rightarrow e^+e^-}$ . The obtained values using the quark masses of  $m_f = 0.03$  GeV for the  $\rho$ ,  $m_f = 1.3$  GeV for  $J/\psi$ ,  $\psi(2S)$ , and  $m_f = 4.2$  GeV for  $\Upsilon$  are given in Table II along with the predicted and measured decay widths of those mesons.

Numerical predictions for exclusive vector meson photoproduction and electroproduction depend on the choice of the vector-meson wave function. One of the authors (M.V.T.M.) has been already involved in the analysis of this type of theoretical uncertainty in Refs. [67–69]. Actually, the change in the meson wavefunction parametrization, given the same model of dipole cross-section, modifies the overall normalization. The effect becomes of more importance for lighter mesons, where the normalization variation becomes quite pronounced.

The light photoproduction is dominated by the non-perturbative (soft) sector, and the confinement effects are significant. This feature can be embedded into the photon wave function by replacing its original form with [70–72]

$$\psi_{T,L}^f(Q, r, z) \rightarrow \sqrt{f_s(r)} \psi_{T,L}^f(Q, r, z), \quad f_s(r) = \frac{1 + B \exp(-\omega^2(r-R)^2)}{1 + B \exp(-\omega^2 R^2)}, \quad (21)$$

where the parameters  $B$ ,  $\omega$ , and  $R$  are determined by fitting the total photoproduction cross-section,  $\sigma(\gamma p \rightarrow X)$ . The shifted Gaussian function  $f_s(r)$  in Equation (21) controls the width and height of the soft contribution enhancement for the photon wavefunction. Moreover,  $f_s \rightarrow 1$  for relatively small dipoles, and then the hard contribution is unchanged. In what follows, we consider the optimal set of parameters for the IPSAT model in the case of  $\rho$  photoproduction:  $B = -0.75$ ,  $\omega = 0.25$  GeV, and  $R = 6.8$  GeV $^{-1}$  (fixed) [72].

Let us move now to the nuclear color dipole amplitude. In this paper, we consider the Glauber–Gribov approach [73–75]. Therefore, the amplitude describing the interaction of the color dipole with a large enough ( $A > 40$ ) nucleus at a fixed impact parameter,  $b$ , is given by [76]

$$\frac{d\sigma_{q\bar{q}}^A}{d^2\vec{b}} = 2 \left[1 - \exp\left(-\frac{1}{2} AT_A(b) \hat{\sigma}(x, \vec{r})\right)\right], \quad (22)$$

where the quantity  $A$  denotes the atomic mass number and  $\sigma(x, \vec{r})$  denotes the dipole–proton cross-section. The underlying physical assumption in Equation (22) is that multiple scattering occurs on individual nucleons, as described by the saturating form in Equation (6).

For nuclear targets, the thickness function is to be obtained from the Woods–Saxon distribution [77] for the nuclear density [78],  $\rho_A(\vec{s}, z)$ , as follows:

$$T_A(b) = \int_{-\infty}^{\infty} dz \rho_A(\vec{b}, z), \quad \int d^2\vec{b} T_A(b) = 1, \quad (23)$$

$$\rho_A(\vec{s}, z) = \frac{\rho_0}{1 + \exp\left(\frac{r - R_A}{d}\right)}, \quad r = \sqrt{\vec{s}^2 + z^2} \quad (24)$$

which is quite a good approximation for nuclei with  $A \geq 4$ . Here,  $\vec{s}$  denotes the transverse distance relative to  $z$  direction, the parameter  $\rho_0$  denotes the density at the center of the nucleus, and, for heavy nuclei, the nuclear

radius  $R_A \simeq 1.12A^{1/3}$  fm and the skin depth  $d = 0.54$  fm are commonly taken from high-energy electron scattering measurements [78].

As a final remark on the theoretical approach considered in the present study, to say is that recently, it has been a considerable progress reached with the NLO calculations within the dipole framework. It might be timely to discuss how those findings affect the results presented here. By comparing the phenomenology of vector mesons production with the NLO CGC calculations [19, 79], one finds significant deviations only in some regions of the phase space (e.g., at relatively low photon-nucleon center-of-mass energy  $W$  for fixed  $Q^2$ ). However, it is quite a complicated task to distinguish between the LO and NLO results, given the data accuracy for vector meson production. Another essential point is that the NLO predictions are available only for protons, and no numerical results are available for nuclear targets so far.

In Section III just below, we apply the obtained cross-section for vector meson photoproduction in  $\gamma A$  scattering to the corresponding coherent production in  $AA$  collisions. The associated rapidity distributions are also investigated.

### III. RESULTS AND DISCUSSIONS

Let us start by calculating the rapidity distribution for coherent vector meson production in proton-proton collisions. The equivalent photon approximation (EPA) is to be used. Thus, the production cross-section in hadron-hadron collisions is factorized as a convolution of photon flux,  $dN_\gamma^p/d\omega$ , and the photoproduction cross-section,  $\sigma(\gamma p \rightarrow Vp)$ . The rapidity distribution of the process  $pp \rightarrow pVp$  is given by the following [36–40]:

$$\frac{d\sigma^{pp}}{dy} = \left[ \mathcal{S}_{\text{gap}}^2(\omega^-) \omega^- \frac{dN_\gamma^p(\omega^-)}{d\omega} \sigma^{\gamma p \rightarrow Vp}(\omega^-) \right] + \left[ \mathcal{S}_{\text{gap}}^2(\omega^+) \omega^+ \frac{dN_\gamma^p(\omega^+)}{d\omega} \sigma^{\gamma p \rightarrow Vp}(\omega^+) \right], \quad (25)$$

where  $\omega^\pm \approx (M_V/2)e^{\pm y}$  accounts for the source-target symmetry appearing in  $pp$  collisions, where each proton simultaneously acts as a source and target of photons.  $\mathcal{S}_{\text{gap}}^2(\omega)$  denotes the rapidity gap survival factor in  $pp$  collisions. In our numerical calculations, the photon flux from a proton is given by the dipole formula for the electric form factor [80]:

$$\frac{dN_\gamma^p(\omega)}{d\omega} = \frac{\alpha}{2\pi\omega} \left[ 1 + \left( 1 - \frac{2\omega}{\sqrt{s_{NN}}} \right)^2 \right] \left( \ln \Omega - \frac{11}{6} + \frac{3}{\Omega} - \frac{3}{2\Omega^2} + \frac{1}{3\Omega^3} \right), \quad (26)$$

where  $s_{NN}$  is the energy squared in the nucleon-nucleon center-of-mass (c.m.),  $\Omega = 1 + 0.71 \text{ GeV}^2/Q_{\text{min}}^2$  and the minimum momentum transferred  $Q_{\text{min}}^2 = \omega^2/[\gamma^2(1 - 2\omega/\sqrt{s_{NN}})] \approx \omega^2/\gamma^2$ , energy). where here  $\gamma = \sqrt{s_{NN}}/2m_N$  represents the Lorentz factor of a single beam. Then, the  $\gamma p$  c.m. energy is  $W_{\gamma p} \simeq \sqrt{2\omega\sqrt{s_{NN}}}$ .

In Figure 1, the results for  $J/\psi$  and  $\psi(2S)$  photoproduction in  $pp$  collisions at the collision c.m. energy  $\sqrt{s} = 13$  TeV (with the data by the LHCb Collaboration [81]) are presented, taking into account the boosted Gaussian wavefunction and our results for the IPSAT model (solid line). The rapidity gap survival factor  $\mathcal{S}_{\text{gap}}^2$  is taken from Ref. [82]. In Figure 1a, the shape of the distribution for  $J/\psi$  overestimates the data at forward rapidities. However, the overall normalization overestimates the data mostly at very forward rapidities in this case. The reason can be traced back to the  $\gamma p \rightarrow J/\psi + p$  cross-section within the same model, which overestimates the extracted high-energy LHCb data [41], while accurately describing the data points at low and intermediate energies. Regarding the  $\psi(2S)$  meson photoproduction, as shown in Figure 1b, the calculation is straightforward as the wavefunctions for excited states are known in the boosted Gaussian parametrization (see Equations (19) and (20)). In this case, the data description is improved with respect to the bound state.

For  $pA$  collisions, following the convention that the nucleon is incident from the right and the nucleus from the left, the rapidity distribution of process  $pA \rightarrow pVA$  reads

$$\frac{d\sigma^{pA}}{dy} = \left[ \omega^- \frac{dN_\gamma^A(\omega^-)}{d\omega} \sigma^{\gamma p \rightarrow Vp}(\omega^-) \right] + \left[ \omega^+ \frac{dN_\gamma^p(\omega^+)}{d\omega} \sigma^{\gamma A \rightarrow VA}(\omega^+) \right], \quad (27)$$

where  $\omega^-$  and  $\omega^+$  address photons from the nucleus and proton, respectively. Here, a reliable analytic approximation for ultraperipheral  $AB$  collisions is given by the photon flux integrated over radii larger than that covered by the nuclei,  $R_A + R_B$ . The numerical result, considering an extended nucleus (described by the nuclear form factor), yields

a harder photon spectrum for heavy nuclei at the same photon energy. Regarding  $pA$  collisions, the flux from the nucleus with charge  $Z$  and atomic mass number  $A$  is evaluated analytically and given by [36]

$$\frac{dN_\gamma^A(\omega)}{d\omega} = \frac{2Z^2\alpha}{\pi\omega} \left[ \xi^{pA} K_0(\xi^{pA}) K_1(\xi^{pA}) - \frac{(\xi^{pA})^2}{2} (K_1^2(\xi^{pA}) - K_0^2(\xi^{pA})) \right], \quad (28)$$

where the parameter  $\xi^{pA}$  is given by  $\xi^{pA} = \omega(R_p + R_A)/\gamma$ , with  $R_p$  the effective radius of the proton. For the photon flux in  $AA$  collisions, in Equation (30), it is to replace  $\xi^{pA} \rightarrow \xi^{AA} = \omega(2R_A)/\gamma$ .

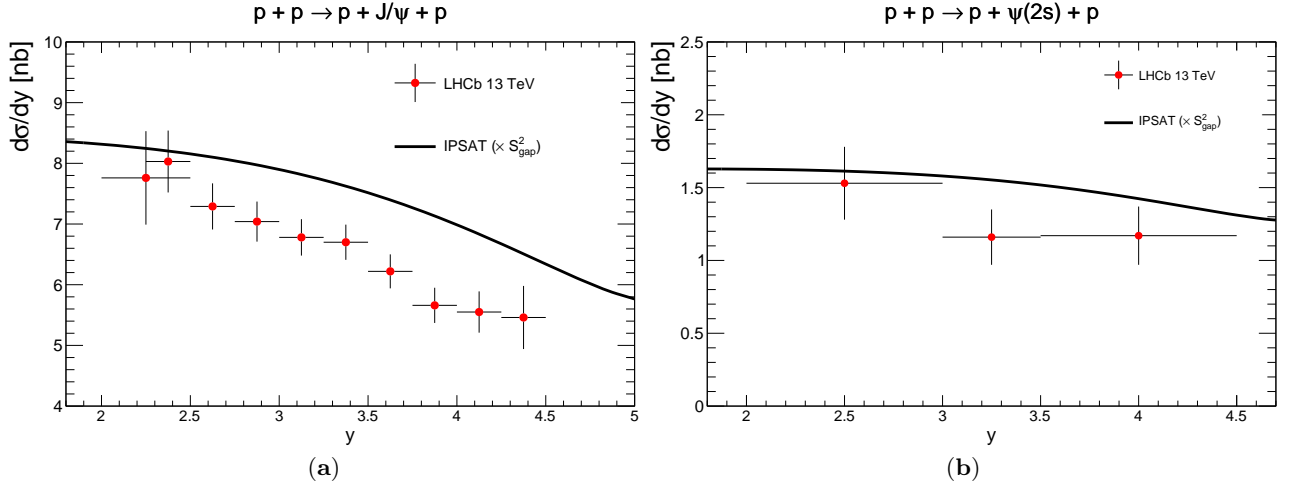


FIG. 1: Comparison of the model (solid line) and the data (dots) for the rapidity distribution for  $J/\psi$  (a) and  $\psi(2S)$  (b) photoproduction in proton–proton collisions at the collision center-of-mass (c.m.) energy of 13 TeV. The model represents our prediction using the IPSAT model with the boosted Gaussian wavefunction (see text for details). The data are the LHCb Collaboration measurements [81].

Let us now move to coherent meson production in ultraperipheral proton–nucleus collisions. Theoretical predictions are compared to the ALICE Collaboration data on charmonium production [83, 84] and the CMS data on bottomonium production Collaboration [85] in  $pPb$  collisions at  $\sqrt{s_{NN}} = 5.02$  TeV. Figure 2a presents the rapidity distribution for the  $J/\psi$  production, whereas Figure 2b shows the corresponding distribution for  $\Upsilon$  production. The role of the rapidity gap survival factor in  $pA$  collisions is investigated for the  $J/\psi$  case. The average  $S_{\text{gap}}^2$  is taken from Ref. [86]. The main effect of including this rapidity interval is the overall normalization. The prediction without the survival factor is also given for the  $\Upsilon$  photoproduction in Figure 2b. The prediction is computed by using the  $\gamma + p \rightarrow \Upsilon + p$  cross-section shown in Figure 3b. The data description in this case is exceptionally good. The inclusion of absorption corrections in ultraperipheral  $pPb$  collisions is obtained to describe the data in a more satisfactory way.

Finally, in  $AA$  collisions, the rapidity distribution of the process  $AA \rightarrow AVA$  reads:

$$\frac{d\sigma^{AA}}{dy} = \left[ \omega^- \frac{dN_\gamma^A(\omega^-)}{d\omega} \sigma^{\gamma A \rightarrow VA}(\omega^-) \right] + \left[ \omega^+ \frac{dN_\gamma^A(\omega^+)}{d\omega} \sigma^{\gamma A \rightarrow VA}(\omega^+) \right], \quad (29)$$

with  $\omega^-$  and  $\omega^+$  just denoting equivalent photons from the nucleus incident from the left and right, respectively. The flux from the nucleus with the charge  $Z$  and atomic mass number  $A$  is evaluated analytically and is given by [36]

$$\frac{dN_\gamma^A(\omega)}{d\omega} = \frac{2Z^2\alpha}{\pi\omega} \left[ \xi K_0(\xi) K_1(\xi) - \frac{(\xi)^2}{2} (K_1^2(\xi) - K_0^2(\xi)) \right], \quad (30)$$

where  $\xi = 2\omega R_A/\gamma$ .

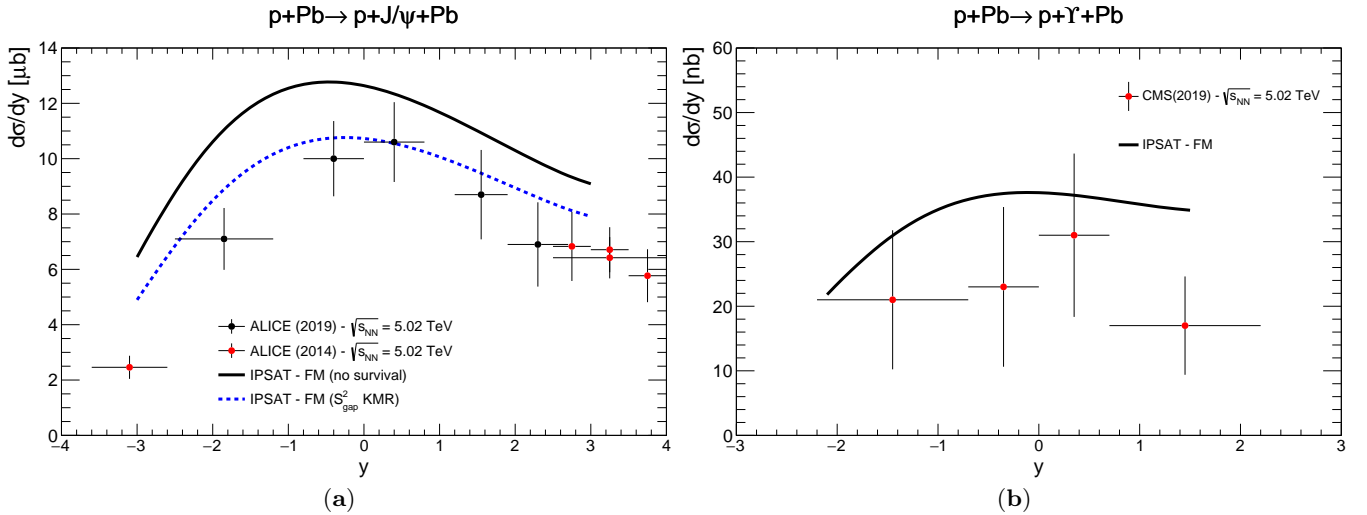


FIG. 2: Comparison of the models (lines) and the data (markers) for the rapidity distribution for  $J/\psi$  (a) and  $\Upsilon$  (b) photoproduction in proton–lead collisions at the nucleon–nucleon c.m. energy of 5.02 TeV. The model represents our predictions using the IPSAT model with the boosted Gaussian wavefunction implemented, without (solid line) and with (dashed line) inclusion of rapidity gap survival suppression (see text for details). The data are the measurements of the ALICE [83, 84] and CMS [85] Collaborations, as indicated.

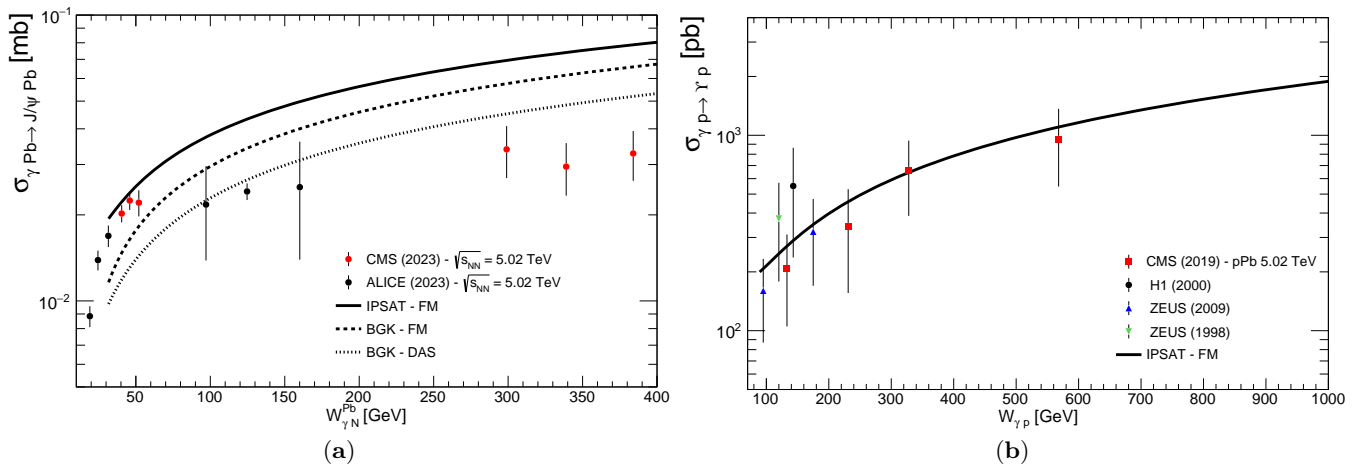


FIG. 3: Comparison of the models (lines) and the data (markers) for the photonuclear cross-section  $\gamma + Pb \rightarrow J/\psi + Pb$  (a) and  $\gamma + Pb \rightarrow \Upsilon + p$  (b) as a function of the photon–nucleon c.m. energy,  $W_{\gamma N}$ . The models represent the predictions using the IPSAT (solid line), BGK (dashed line), and the BGK-DAS (dotted line) models (see text for details). The data are the measurements by the CMS Collaboration in PbPb collisions [87] and the ALICE Collaboration in  $pPb$  collisions [83, 84] at the nucleon–nucleon c.m. energy of 5.02 TeV (a) and of the CMS Collaboration in  $pPb$  collisions at the nucleon–nucleon c.m. energy of 5.02 TeV [85] and the H1 [88] and ZEUS [89, 90] Collaborations in  $ep$  collisions at the photon–proton c.m. energy  $26 < W < 300$  GeV (b), as indicated.

Now, we address the photonuclear production of vector mesons in  $AA$  collisions at colliders. First, let us consider PbPb and XeXe collisions at LHC at the  $NN$  c.m. energies of 5.02 TeV and 5.44 TeV, respectively. First, let us focus on the coherent production without nuclear breakup. In Figure 3a, we present the result concerning the photonuclear cross-section,  $\gamma + Pb \rightarrow J/\psi + Pb$ , as a function of  $W_{\gamma N}$ , and considering the boosted Gaussian wavefunction and the IPSAT, BGK, and BGK-DAS. One finds that the IPSAT and BGK models are consistent with the low-energy data but produce predictions that overestimate the data [87] at  $W_{\gamma N}$  above 300 GeV. In Figure 4a, the results for the coherent  $J/\psi$  production,  $Pb + Pb \rightarrow Pb + J/\psi + Pb$ , are shown. The rapidity distributions are present in both central and forward rapidity regions. The change in the overall normalization follows the results of the photonuclear cross-section, as shown in Figure 4a. That is, the models overestimate the data at high c.m. energies (very forward/backward rapidities). Certainly, there is a normalization discrepancy between the ALICE [91, 92] and LHCb [93] Collaborations data what remains a matter of discussion. Furthermore, a significant suppression in the data relative to theoretical

predictions persists at central rapidities. In the literature, within the context of the color dipole picture, this issue can be solved by including contributions from the next Fock states of the virtual photon,  $q\bar{q}(ng)$  (with  $n = 1, 2, \dots$  and  $g$  denoting the gluon) [23, 94–99]. These corrections are directly related to the gluon nuclear shadowing phenomenon, as discussed in Refs. [23, 98, 99] and in the references therein. It is worth mentioning that the finite coherence length corrections [23, 96, 99] are not included in the present calculations. For completeness, the analysis for coherent  $\rho^0$  production in PbPb collisions is presented in Figure 4b in comparison to the ALICE Collaboration data [100]. A weaker model-dependence compared to the  $J/\psi$  is verified. This can be related to the universal behavior of the dipole cross-section,  $N(r \gg 1/Q_s) \rightarrow 1$ , for large dipoles, which dominate the dynamics for light meson photoproduction. The cross-section for the nucleon target,  $\gamma + p \rightarrow \rho^0 + p$ , was described by us earlier in Ref. [41]. The coherent  $\rho$ -production in XeXe collisions is presented in Figure 5 and compared with the ALICE Collaboration data [101]. The results follow a trend similar to that of the PbPb collision case.

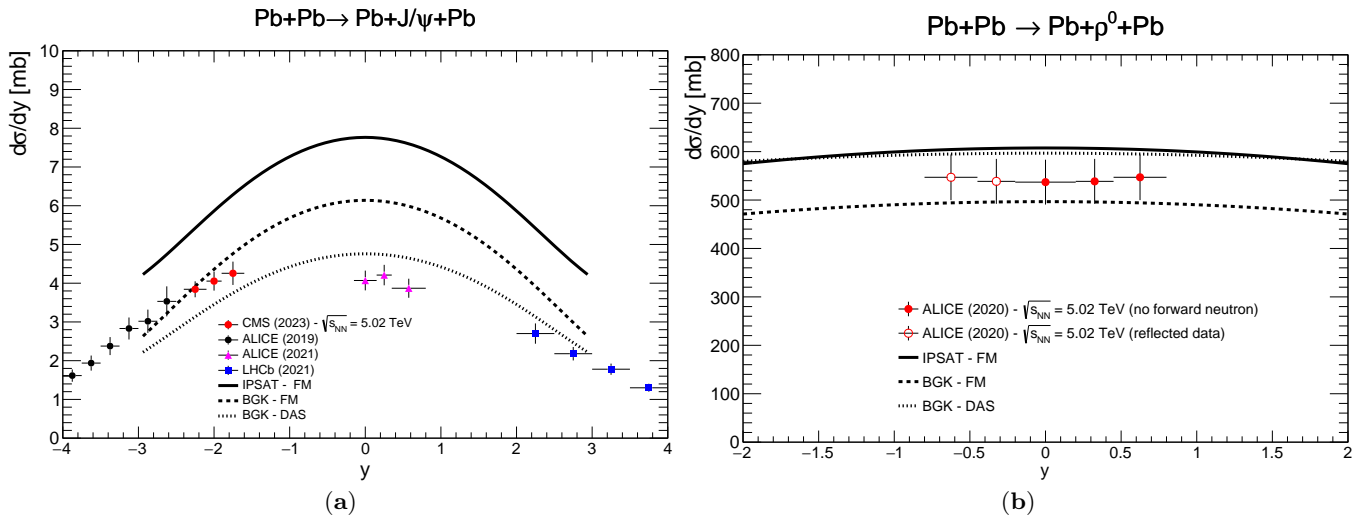


FIG. 4: Comparison of the models (lines) and data (markers) for the rapidity distributions of coherent  $J/\psi$  (a) and  $\rho^0$  (b) production in PbPb collisions at the nucleon–nucleon c.m. energy of 5.02 GeV. The models represent the predictions using the IPSAT (solid line), BGK (dashed line), and the BGK-DAS (dotted line) models (see text for details). The data are the measurements by the ALICE [91, 92], LHCb [93], and CMS [87] Collaborations (a) and by the ALICE Collaboration [100] (b), as indicated.

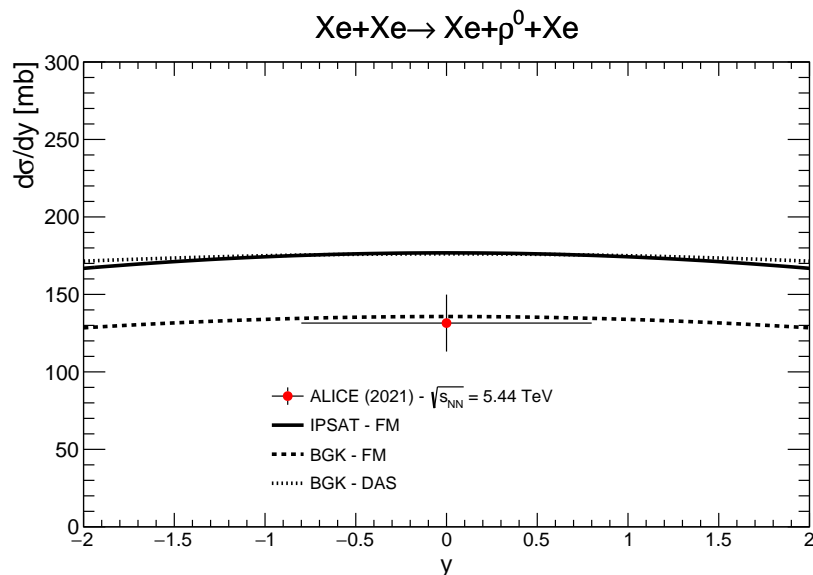


FIG. 5: Comparison of the models (lines) and data (dot) for the rapidity distribution of the coherent photoproduction of  $\rho^0$  mesons in XeXe UPC at midrapidity at the nucleon–nucleon c.m. energy of 5.44 TeV. Predictions of the IPSAT (solid line), BGK (dashed line), and the BGK-DAS (dotted line) models are compared with the data by the ALICE Collaboration [101].

Regarding the predictions for light mesons, some comments are in order. The DAS parametrization (and its modification proposed here) for the gluon density is valid in the  $x \rightarrow 0$  and  $Q^2 \rightarrow \infty$  limits. In light of meson photoproduction, there is no hard scale, and the validity of the approach in this case could be questioned. The answer to this question was already given in our earlier study [41], where we were able to describe the data from the proton structure function  $F_2$  to considerably low  $Q^2$ , the total photoabsorption cross-section, and the  $\rho$  photoproduction itself using the dipole-DAS-based models. The point is that the agreement with the data is not related to the gluon distribution at that  $Q^2$ -scale, but rather to the multiple scattering effects embedded in the IP-SAT or BGK models. On scales below pQCD validity  $\mu \lesssim 1$  GeV, the wavefunction overlap selects large-dipole configurations, for which the cross-section becomes essentially constant in these eikonal-based models, independent of the behavior of the gluon distribution at such low scales.

Finally, let us address the Coulomb nuclear breakup. In this process, the nuclei participating undergoes electromagnetic dissociation (EMD), producing neutrons [102]. The cross-section for a symmetric ultraperipheral  $AA$  collision accompanied by the breakup of one or both nuclei, with the production of a vector meson is given by [103, 104]:

$$\sigma(AA \rightarrow VA'_i A'_j) \propto \int d^2\vec{b} \int d\omega \frac{d^2n(\omega, b)}{d\omega d^2\vec{b}} \sigma_{\gamma A \rightarrow VA}(\omega) P_{ij}(b) \exp[-P_H(b)], \quad (31)$$

where  $P_{ij}(b) = P_i(b) \times P_j(b)$  denotes the probability of nuclear breakup with emissions of  $i$  and  $j$  neutrons ( $i, j = 0, 1, 2, \dots$ ), respectively, from the first and second nucleus, and  $P_H(b) = \int d^2\vec{r} T_A(\vec{r} - \vec{b}) [1 - \exp(-\sigma_{NN} T_A(\vec{r}))]$  denotes the probability of a hadronic interaction with the inelastic  $NN$  cross-section at the corresponding c.m. energy,  $\sigma_{NN}(\sqrt{s_{NN}})$ . In the EPA approximation, the flux of photons,  $d^2n/d\omega d^2\vec{b}$ , produced with energy  $\omega$  at impact parameter  $\vec{b}$ , can be expressed by the following:

$$\frac{d^2n(\omega, b)}{d\omega d^2\vec{b}} = \frac{Z^2\alpha}{\pi^2\gamma^2} \omega \left[ k_1^2(\zeta) + \frac{1}{\gamma^2} k_0^2(\zeta) \right], \quad \zeta = \frac{\omega b}{\gamma}. \quad (32)$$

In our numerical calculations, in what follows, the Monte Carlo program **n<sup>o</sup>n** (noon) [103] of forward neutrons for UPC was used. The program is a ROOT-based code that can be interfaced with existing generators of exclusive vector meson production in UPC or with theoretical calculations of such processes. Setting the notation,  $P_{Xn}$  denotes the probability of the nuclear breakup of one nucleus to a state with any number ( $X$ ) of neutrons ( $n$ ).  $P_{Xn}$  is obtained through the mean number of the Coulomb excitation of the nucleus to any state that emits one or more neutrons,  $P_{Xn}^1$ . In Figure 6a, the rapidity distributions from coherent  $J/\psi$  production in  $0n0n$ ,  $0nXn$ , and  $XnXn$  neutron multiplicity classes are presented and contrasted to the experimental measurements by the CMS [87] and ALICE Collaborations [105]. Theoretical predictions are also given in each class for the IPSAT, BGK, and BGK-DAS models. One finds that at large rapidities, the deviations among the models are quite similar to the predictions without the EMD effect. The BGK model produces better describes the data in the  $0n0n$  and  $0nXn$  classes, whereas BGK-DAS provides better agreed results for the  $XnXn$  class in the case of the CMS experiment dataset. When both experimental datasets are considered, the overall normalization is well enough described within the theoretical uncertainties (comparing the three implementations of the nuclear dipole amplitude). In effect, given its higher normalization, IPSAT shall be regarded hereafter as an upper bound of the dipole amplitude for  $J/\psi$  photoproduction, while the BGK-DAS model as the lower bound. The rapidity distribution for  $\rho^0$ -production in the same neutron multiplicity classes is shown in Figure 6b. The predictions are compared to the measurements by the ALICE Collaboration [100]. As already discussed above in this Section, in the case without nuclear breakup, the difference among the models is less pronounced in the light-meson photoproduction.

Lastly, let us consider the quite recent RHIC measurements on  $J/\psi$  production in AuAu collisions at 200 GeV [106], for neutron multiplicity classes  $0n0n$ ,  $0nXn$ , and  $XnXn$ . The calculations compared to those measurements are shown in Figure 7, which, to be said not quite unexpectedly, demonstrate that all data points fall within the uncertainty region previously defined by the IPSAT (upper bound) and BGK-DAS (lower bound) models.

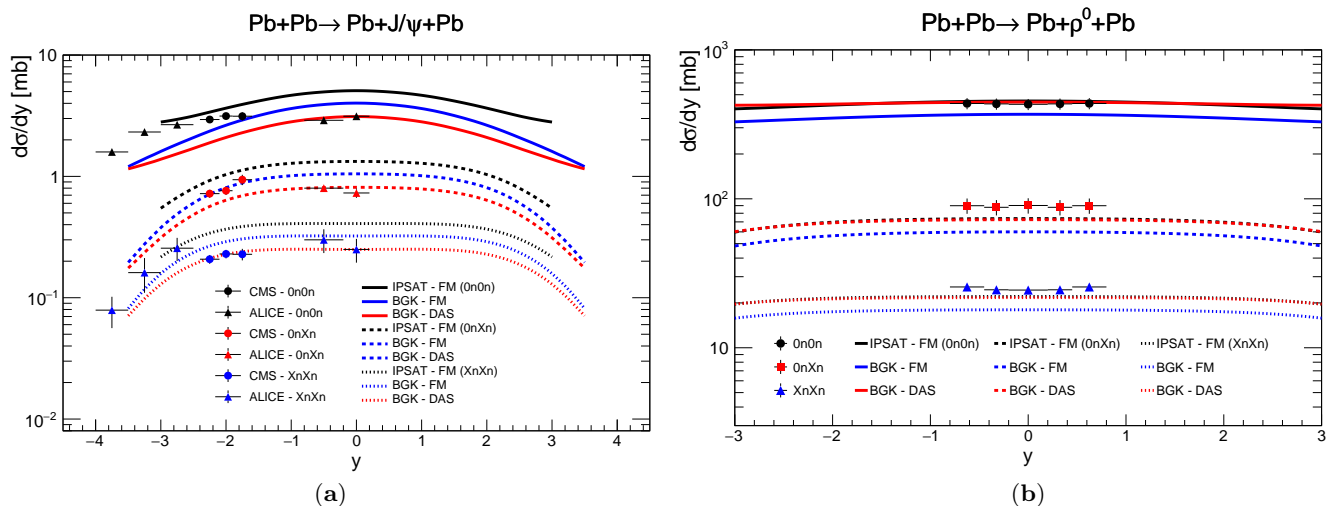


FIG. 6: Comparison of the models (lines) and the data (markers) for the rapidity distribution for coherent  $J/\psi$  (a) and  $\rho^0$  (b) photoproduction in PbPb collisions at the nucleon–nucleon c.m. energy of 5.02 GeV in three neutron multiplicity classes. Theoretical predictions from the IPSAT (upper), BGK (middle), and BGK-DAS (lower) models for 0n0n (solid lines), 0nXn (dashed lines), and XnXn (dotted lines) classes (see text for details) are compared with the measurements by the CMS [87] and ALICE [105] Collaborations (a) and by the ALICE Collaboration [100] (b), as indicated.

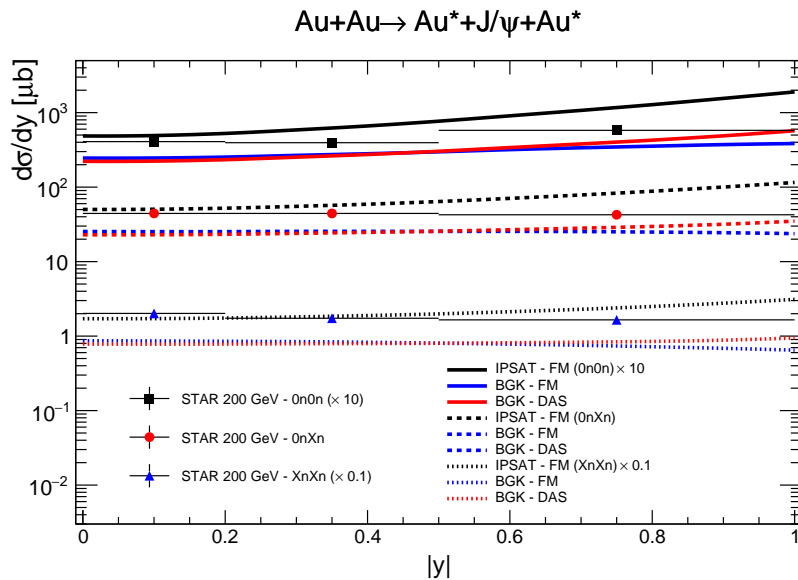


FIG. 7: Comparison of the models (lines) and the data (markers) for the rapidity distribution of coherent  $J/\psi$  production in AuAu collisions at 200 GeV in three neutron multiplicity classes. Theoretical predictions from the IPSAT (upper), BGK (middle), and BGK-DAS (lower) models for 0n0n (solid lines), 0nXn (dashed lines), and XnXn (dotted lines) classes (see text for details) are compared with the measurements by the STAR Collaboration [106], as indicated.

#### IV. CONCLUSIONS AND FINAL REMARKS

In summary, in this paper, the calculations have been performed considering an analytical gluon distribution based on DAS approximation, leading to predictions for the exclusive vector meson production of  $\rho^0$ ,  $J/\psi$ ,  $\psi(2S)$ , and  $\Upsilon(1S)$ . The focus is on their coherent production of the mesons in  $pp$ ,  $pA$ , and  $AA$  collisions at the LHC and RHIC energies. This analysis extended the investigation presented earlier in Ref. [41], where the models were proposed and compared to structure functions and exclusive meson production in the HERA kinematics. It is shown that the different implementations of the dipole–proton amplitude (IPSAT-FM, BGK-FM, and BGK-DAS) using such a gluon PDF lead to a sizable theoretical uncertainty in the photonuclear cross-section and rapidity distributions. Certainly,

other sources of uncertainties, such as the meson wave function and quark masses in the phenomenological models, are not addressed at this stage. In numerical calculations, the boosted Gaussian meson wavefunction was used; a change in the normalization of the rapidity distributions is expected when other parametrizations are considered, such as the light-cone Gaussian (LCG). In general, the rapidity distributions of coherent vector-meson production are obtained to be fairly well described by the analytical gluon PDF. The electromagnetic dissociation in nucleus–nucleus collisions has also been studied. Based on the  $n_{\text{O}}n$  generator, the rapidity distributions for coherent meson photoproduction in  $0n0n$ ,  $0nXn$ , and  $XnXn$  neutron multiplicity classes have been computed. Taking into account the theoretical uncertainty, the models are found to be able to describe the recent LHC data for  $J/\psi$  and  $\rho^0$  production and the recent RHIC-STAR data.

### Acknowledgments

We thank Christopher Flett for discussions on the survival probability in  $pA$ . DAF acknowledges the support of the project INCT-FNA (464898/2014-5), Brazil. MVTM was supported by funding agencies CAPES (Finance Code 001) and CNPq (grant number 303075/2022-8), Brazil.

- 
- [1] Gribov, L.V.; Levin, E.M.; Ryskin, M.G. Semihard processes in QCD. *Phys. Rep.* **1983**, *100*, 1–150. [CrossRef]
  - [2] Mueller, A.H.; Qiu, J.W. Gluon recombination and shadowing at small values of  $x$ . *Nucl. Phys. B* **1986**, *268*, 427–452. [CrossRef]
  - [3] Mueller, A.H. Parton saturation: An overview. In Proceedings of the Cargese Summer School on QCD Perspectives on Hot and Dense Matter, Cargese, France, 6–18 August 2001; pp. 45–72. [CrossRef]
  - [4] McLerran, L.D.; Venugopalan, R. Computing quark and gluon distribution functions for very large nuclei. *Phys. Rev. D* **1994**, *49*, 2233–2241. [CrossRef]
  - [5] McLerran, L.D.; Venugopalan, R. Gluon distribution functions for very large nuclei at small transverse momentum. *Phys. Rev. D* **1994**, *49*, 3352–3355. [CrossRef]
  - [6] McLerran, L.D.; Venugopalan, R. Green’s functions in the color field of a large nucleus. *Phys. Rev. D* **1994**, *50*, 2225–2233. [CrossRef]
  - [7] Ayala, A.; Jalilian-Marian, J.; McLerran, L.D.; Venugopalan, R. The gluon propagator in non-Abelian Weizsäcker–Williams fields. *Phys. Rev. D* **1995**, *52*, 2935–2943. [CrossRef]
  - [8] Ayala, A.; Jalilian-Marian, J.; McLerran, L.D.; Venugopalan, R. Quantum corrections to the Weizsäcker–Williams gluon distribution function at small  $x$ . *Phys. Rev. D* **1996**, *53*, 458–475. [CrossRef]
  - [9] Iancu, E.; Venugopalan, R. The color glass condensate and high energy scattering in QCD. In *Quark–Gluon Plasma 3*; Hwa, R.C., Wang, X.-N., Eds.; World Scientific Co. Ltd.: Singapore, 2004; pp. 249–363. [CrossRef]
  - [10] Gelis, F.; Iancu, E.; Jalilian-Marian, J.; Venugopalan, R. The Color Glass Condensate. *Ann. Rev. Nucl. Part. Sci.* **2010**, *60*, 463–489. [CrossRef]
  - [11] Morreale, A.; Salazar, F. Mining for Gluon Saturation at Colliders. *Universe* **2021**, *7*, 312. [CrossRef]
  - [12] Nikolaev, N.N.; Zakharov, B.G. Color transparency and scaling properties of nuclear shadowing in deep inelastic scattering. *Z. Phys. C* **1991**, *49*, 607–618. [CrossRef]
  - [13] Nikolaev, N.N.; Zakharov, B.G. Pomeron structure function and diffraction dissociation of virtual photons in perturbative QCD. *Z. Phys. C* **1992**, *53*, 331–346. [CrossRef]
  - [14] Mueller, A.H. Soft gluons in the infinite momentum wave function and the BFKL pomeron. *Nucl. Phys. B* **1994**, *415*, 373–385. [CrossRef]
  - [15] Mueller, A.H.; Patel, B. Single and double BFKL pomeron exchange and a dipole picture of high-energy hard processes. *Nucl. Phys. B* **1994**, *425*, 471–488. [CrossRef]
  - [16] Henkels, C.; de Oliveira, E.G.; Pasechnik, R.; Trebien, H. Exclusive photo- and electroproduction of excited light vector mesons via holographic model. *Eur. Phys. J. C* **2023**, *83*, 551. [CrossRef]
  - [17] Cisek, A.; Schäfer, W.; Szczurek, A. Exclusive production of  $\rho$  meson in gamma-proton collisions:  $d\sigma/dt$  and the role of helicity flip processes. *Phys. Lett. B* **2023**, *836*, 137595. [CrossRef]
  - [18] Mäntysaari, H.; Salazar, F.; Schenke, B. Nuclear geometry at high energy from exclusive vector meson production. *Phys. Rev. D* **2022**, *106*, 074019. [CrossRef]
  - [19] Mäntysaari, H.; Penttala, J. Complete calculation of exclusive heavy vector meson production at next-to-leading order in the dipole picture. *J. High Energy Phys.* **2022**, *2022*, 247. [CrossRef]
  - [20] Mäntysaari, H.; Penttala, J. Exclusive production of light vector mesons at next-to-leading order in the dipole picture. *Phys. Rev. D* **2022**, *105*, 114038. [CrossRef]
  - [21] Mäntysaari, H.; Penttala, J. Exclusive heavy vector meson production at next-to-leading order in the dipole picture. *Phys. Lett. B* **2021**, *823*, 136723. [CrossRef]
  - [22] Kopeliovich, B.Z.; Krelina, M.; Nemchik, J. Electroproduction of heavy quarkonia: Significance of dipole orientation. *Phys. Rev. D* **2021**, *103*, 094027. [CrossRef]

- [23] Kopeliovich, B.Z.; Krelina, M.; Nemchik, J.; Potashnikova, I.K. Coherent photoproduction of heavy quarkonia on nuclei. *Phys. Rev. D* **2022**, *105*, 054023. [CrossRef]
- [24] Cepila, J.; Contreras, J.G.; Vaculciak, M. Solutions to the Balitsky–Kovchegov equation including the dipole orientation. *Phys. Lett. B* **2024**, *848*, 138360. [CrossRef]
- [25] Matousek, G.; Khachatryan, V.; Zhang, J. Scaling properties of exclusive vector meson production cross section from gluon saturation. *Eur. Phys. J. Plus* **2023**, *138*, 113. [CrossRef]
- [26] Kumar, A.; Toll, T. Energy dependence of the proton geometry in exclusive vector meson production. *Phys. Rev. D* **2022**, *105*, 114011. [CrossRef]
- [27] Anand, S.; Toll, T. Exclusive diffractive vector meson production: A comparison between the dipole model and the leading twist shadowing approach. *Phys. Rev. C* **2019**, *100*, 024901. [CrossRef]
- [28] Xie, Y.P.; Goncalves, V.P. Exclusive processes in ep collisions at the EIC and LHeC: A closer look on the predictions of saturation models. *Phys. Rev. D* **2022**, *105*, 014033. [CrossRef]
- [29] Henkels, C.; de Oliveira, E.G.; Pasechnik, R.; Trebien, H. Coherent photoproduction of light vector mesons off nuclear targets in the dipole picture. *Nucl. Phys. A* **2025**, *1055*, 123018. [CrossRef]
- [30] Mäntysaari, H.; Salazar, F.; Schenke, B. Energy dependent nuclear suppression from gluon saturation in exclusive vector meson production. *Phys. Rev. D* **2024**, *109*, L071504. [CrossRef]
- [31] Mäntysaari, H.; Salazar, F.; Schenke, B.; Shen, C.; Zhao, W. Effects of nuclear structure and quantum interference on diffractive vector meson production in ultraperipheral nuclear collisions. *Phys. Rev. C* **2024**, *109*, 024908. [CrossRef]
- [32] Azevedo, C.N.; Goncalves, V.P.; Moreira, B.D. Associated vector-meson and bound-free electron-positron pair photoproduction in ultraperipheral PbPb collisions. *Phys. Rev. C* **2023**, *108*, 064907. [CrossRef]
- [33] Goncalves, V.P.; Klasen, M.; Moreira, B.D. Exclusive  $J/\Psi$  plus jet associated production in ultraperipheral  $PbPb$  collisions. *Eur. Phys. J. C* **2023**, *83*, 895. [CrossRef]
- [34] Boroun, G.R. A simple model for the charm structure function of nuclei. *Phys. Lett. B* **2024**, *849*, 138440. [CrossRef]
- [35] Boroun, G.R. Heavy quark structure functions from unifying the color dipole picture and double asymptotic scaling approaches. *Phys. Rev. D* **2024**, *109*, 054012. [CrossRef]
- [36] Bertulani, C.A.; Baur, G. Electromagnetic processes in relativistic heavy ion collisions. *Phys. Rep.* **1988**, *163*, 299–408. [CrossRef]
- [37] Baur, G.; Hencken, K.; Trautmann, D.; Sadovsky, S.; Kharlov, Y. Coherent  $\gamma\gamma$  and  $\gamma A$  interactions in very peripheral collisions at relativistic ion colliders. *Phys. Rep.* **2002**, *364*, 359–450. [CrossRef]
- [38] Bertulani, C.A.; Klein, S.R.; Nystrand, J. Physics of ultra-peripheral nuclear collisions. *Ann. Rev. Nucl. Part. Sci.* **2005**, *55*, 271–310. [CrossRef]
- [39] Baltz, A.J.; Baur, G.; d’Enterria, D.; Frankfurt, L.; Gelis, F.; Guzey, V.; Hencken, K.; Kharlov, Y.; Klasen, M.; Klein, S.R.; et al. The physics of ultraperipheral collisions at the LHC. *Phys. Rep.* **2008**, *458*, 1–171. [CrossRef]
- [40] Klein, S.; Steinberg, P. Photonuclear and two-photon interactions at high-energy nuclear colliders. *Ann. Rev. Nucl. Part. Sci.* **2020**, *70*, 323–354. [CrossRef]
- [41] Fagundes, D.A.; Machado, M.V.T. Asymptotic gluon density within the color dipole picture in light of HERA high-precision data. *Phys. Rev. D* **2023**, *107*, 014004. [CrossRef]
- [42] Caola, F.; Forte, S. Geometric scaling from GLAP evolution. *Phys. Rev. Lett.* **2008**, *101*, 022001. [CrossRef]
- [43] Ball, R.D.; Nocera, E.R.; Rojo, J. The asymptotic behaviour of parton distributions at small and large  $x$ . *Eur. Phys. J. C* **2016**, *76*, 383. [CrossRef]
- [44] Rezaeian, A.H.; Schmidt, I. Impact-parameter dependent color glass condensate dipole model and new combined HERA data. *Phys. Rev. D* **2013**, *88*, 074016. [CrossRef]
- [45] Mäntysaari, H.; Zurita, P. In depth analysis of the combined HERA data in the dipole models with and without saturation. *Phys. Rev. D* **2018**, *98*, 036002. [CrossRef]
- [46] Ball, R.D.; Forte, S. Double asymptotic scaling at HERA. *Phys. Lett. B* **1994**, *335*, 77–86. [CrossRef]
- [47] Kowalski, H.; Teaney, D. An impact parameter dipole saturation model. *Phys. Rev. D* **2003**, *68*, 114005. [CrossRef]
- [48] Mäntysaari, H.; Schenke, B. Confronting impact parameter dependent JIMWLK evolution with HERA data. *Phys. Rev. D* **2018**, *98*, 034013. [CrossRef]
- [49] Golec-Biernat, K.J.; Wusthoff, M. Saturation effects in deep inelastic scattering at low  $Q^2$  and its implications on diffraction. *Phys. Rev. D* **1998**, *59*, 014017. [CrossRef]
- [50] Golec-Biernat, K.J.; Wusthoff, M. Saturation in diffractive deep inelastic scattering. *Phys. Rev. D* **1999**, *60*, 114023. [CrossRef]
- [51] Bartels, J.; Golec-Biernat, K.J.; Kowalski, H. A modification of the saturation model: DGLAP evolution. *Phys. Rev. D* **2002**, *66*, 014001. [CrossRef]
- [52] Golec-Biernat, K.J.; Sapeta, S. Heavy flavour production in DGLAP improved saturation model. *Phys. Rev. D* **2006**, *74*, 054032. [CrossRef]
- [53] Golec-Biernat, K.; Sapeta, S. Saturation model of DIS: An update. *J. High Energy Phys.* **2018**, *2018*, 102. [CrossRef]
- [54] Luszczak, A.; Luszczak, M.; Schäfer, W. Unintegrated gluon distributions from the color dipole cross section in the BGK saturation model. *Phys. Lett. B* **2022**, *835*, 137582. [CrossRef]
- [55] Boroun, G.R. The unintegrated gluon distribution from the GBW and BGK models. *Eur. Phys. J. A* **2024**, *60*, 48. [CrossRef]
- [56] Kovchegov, Y.V.; Levin, E. *Quantum Chromodynamics at High Energy*; Cambridge University Press: Cambridge, UK, 2013. [CrossRef]
- [57] Kowalski, H.; Motyka, L.; Watt, G. Exclusive diffractive processes at HERA within the dipole picture. *Phys. Rev. D*

- 2006**, *74*, 074016. [CrossRef]
- [58] Shuvaev, A.G.; Golec-Biernat, K.J.; Martin, A.D.; Ryskin, M.G. Off diagonal distributions fixed by diagonal partons at small  $x$  and  $\xi$ . *Phys. Rev. D* **1999**, *60*, 014015. [CrossRef]
- [59] Harland-Lang, L.A. Simple form for the low- $x$  generalized parton distributions in the skewed regime. *Phys. Rev. D* **2013**, *88*, 034029. [CrossRef]
- [60] Favart, L.; Machado, M.V.T.; Schoeffel, L. Extraction of the skewing factor from the DIS/DVCS ratio. *arXiv* **2005**, arXiv:hep-ph/0511069. [CrossRef]
- [61] Favart, L.; Machado, M.V.T.; Schoeffel, L. An extraction of the skewing factor from DESY-HERA data. *Braz. J. Phys.* **2007**, *37*, 798–800. [CrossRef]
- [62] Schoeffel, L. Deeply virtual compton scattering at HERA and perspectives at CERN. *AIP Conf. Proc.* **2008**, *1056*, 372–379. [CrossRef]
- [63] Nemchik, J.; Nikolaev, N.N.; Zakharov, B.G. Scanning the BFKL pomeron in elastic production of vector mesons at HERA. *Phys. Lett. B* **1994**, *341*, 228–237. [CrossRef]
- [64] Nemchik, J.; Nikolaev, N.N.; Predazzi, E.; Zakharov, B.G. Color dipole phenomenology of diffractive electroproduction of light vector mesons at HERA. *Z. Phys. C* **1997**, *75*, 71–87. [CrossRef]
- [65] Cox, B.E.; Forshaw, J.R.; Sandapen, R. Diffractive  $\Upsilon$  production at the Tevatron and LHC. *J. High Energy Phys.* **2009**, *2009*, 34. [CrossRef]
- [66] Armesto, N.; Rezaeian, A.H. Exclusive vector meson production at high energies and gluon saturation. *Phys. Rev. D* **2014**, *90*, 054003. [CrossRef]
- [67] Sampaio dos Santos, G.; Machado, M.V.T. On theoretical uncertainty of color dipole phenomenology in the  $J/\psi$  and  $\Upsilon$  photoproduction in  $pA$  and  $AA$  collisions at the CERN Large Hadron Collider. *J. Phys. G* **2015**, *42*, 105001. [CrossRef]
- [68] Sampaio dos Santos, G.; Machado, M.V.T. Light vector meson photoproduction in hadron–hadron and nucleus–nucleus collisions at energies available at the CERN Large Hadron Collider. *Phys. Rev. C* **2015**, *91*, 025203. [CrossRef]
- [69] Gonçalves, V.P.; Machado, M.V.T.; Moreira, B.D.; Navarra, F.S.; Sampaio dos Santos, G. Color dipole predictions for the exclusive vector meson photoproduction in  $pp$ ,  $pPb$ , and  $PbPb$  collisions at run 2 LHC energies. *Phys. Rev. D* **2017**, *96*, 094027. [CrossRef]
- [70] Frankfurt, L.; Guzey, V.; Strikman, M. Cross section fluctuations of photon projectile in the generalized vector meson dominance model. *Phys. Rev. D* **1998**, *58*, 094039. [CrossRef]
- [71] Forshaw, J.R.; Kerley, G.; Shaw, G. Extracting the dipole cross section from photo- and electroproduction total cross-section data. *Phys. Rev. D* **1999**, *60*, 074012. [CrossRef]
- [72] Gonçalves, V.P.; Moreira, B.D. A phenomenological analysis of the nonperturbative QCD contributions for the photon wave function. *Eur. Phys. J. C* **2020**, *80*, 492. [CrossRef]
- [73] Glauber, R.J. High-energy collision theory. In *Lectures in Theoretical Physics. Volume 1*; Brittin, W.E., Dunham, L.G., Eds.; Interscience Publishers, Inc.: New York, NY, USA; London, UK, 1959; pp. 315–414. Available online: <https://archive.org/details/lecturesintheore0001unse/> (accessed on 31 March 2025).
- [74] Gribov, V.N. Glauber corrections and the interaction between high-energy hadrons and nuclei. *Sov. Phys. JETP* **1969**, *29*, 483–487. Available online: <http://jetp.ras.ru/cgi-bin/e/index/e/29/3/p483?a=list> (accessed on 31 March 2025).
- [75] Gribov, V.N. Interaction of gamma quanta and electrons with nuclei at high energies. *Sov. Phys. JETP*. **1970**, *30*, 709–717. Available online: <http://jetp.ras.ru/cgi-bin/e/index/e/30/4/p709?a=list> (accessed on 31 March 2025).
- [76] Armesto, N. A Simple model for nuclear structure functions at small  $x$  in the dipole picture. *Eur. Phys. J. C* **2002**, *26*, 35–43. [CrossRef]
- [77] Woods, R.D.; Saxon, D.S. Diffuse surface optical model for nucleon–nuclei scattering. *Phys. Rev.* **1954**, *95*, 577–578. [CrossRef]

- [78] De Vries, H.; De Jager, C.; De Vries, C. Nuclear charge-density-distribution parameters from elastic electron scattering. *Atom. Data Nucl. Data Tables* **1987**, *36*, 495–536. [CrossRef]
- [79] Roa, M.; Garrido, J.; Guevara, M. CGC and saturation approach: Impact-parameter dependent model of perturbative QCD and combined HERA data. *Phys. Rev. D* **2024**, *110*, 074006. [CrossRef]
- [80] Drees, M.; Zeppenfeld, D. Production of supersymmetric particles in elastic  $ep$  collisions. *Phys. Rev. D* **1989**, *39*, 2536. [CrossRef]
- [81] Aaij, R. et al. [The LHCb Collaboration] Central exclusive production of  $J/\psi$  and  $\psi(2S)$  mesons in  $pp$  collisions at  $\sqrt{s} = 13$  TeV. *J. High Energy Phys.* **2018**, *2018*, 167. [CrossRef]
- [82] Jones, S.P.; Martin, A.D.; Ryskin, M.G.; Teubner, T. Exclusive  $J/\psi$  production at the LHC in the  $k_T$  factorization approach. *J. Phys. G* **2017**, *44*, 03LT01. [CrossRef]
- [83] Abelev, B.B. et al. [ALICE Collaboration] Exclusive  $J/\psi$  photoproduction off protons in ultraperipheral  $p$ -Pb collisions at  $\sqrt{s_{NN}} = 5.02$  TeV. *Phys. Rev. Lett.* **2014**, *113*, 232504. [CrossRef]
- [84] Acharya, S. et al. [ALICE Collaboration] Energy dependence of exclusive  $J/\psi$  photoproduction off protons in ultraperipheral  $p$ -Pb collisions at  $\sqrt{s_{NN}} = 5.02$  TeV. *Eur. Phys. J. C* **2019**, *79*, 402. [CrossRef]
- [85] Sirunyan, A.M. et al. [CMS Collaboration] Measurement of exclusive  $\Upsilon$  photoproduction from protons in pPb collisions at  $\sqrt{s_{NN}} = 5.02$  TeV. *Eur. Phys. J. C* **2019**, *79*, 277.
- [86] Flett, C.A.; Jones, S.P.; Martin, A.D.; Ryskin, M.G.; Teubner, T. Exclusive  $J/\psi$  and  $\Upsilon$  production in high energy  $pp$  and  $p$ -Pb collisions. *Phys. Rev. D* **2022**, *106*, 074021. [CrossRef]
- [87] Tumasyan, A. et al. [CMS Collaboration] Probing small Bjorken- $x$  nuclear gluonic structure via coherent  $J/\psi$  photoproduction in ultraperipheral Pb-Pb collisions at  $\sqrt{s_{NN}} = 5.02$  TeV. *Phys. Rev. Lett.* **2023**, 262301. . [CrossRef]
- [88] Adloff, C. et al. [H1 Collaboration] Elastic photoproduction of  $J/\psi$  and  $\Upsilon$  mesons at HERA. *Phys. Lett. B* **2000**, *483*, 23–35. [CrossRef]
- [89] Chekanov, S. et al. [ZEUS Collaboration] Exclusive photoproduction of  $\Upsilon$  mesons at HERA. *Phys. Lett. B* **2009**, *680*, 4–12. [CrossRef]
- [90] Breitweg, J. et al. [ZEUS Collaboration] Measurement of elastic  $\Upsilon$  photoproduction at HERA. *Phys. Lett. B* **1998**, *437*, 432–444. [CrossRef]
- [91] Acharya, S. et al. [ALICE Collaboration] Coherent  $J/\psi$  photoproduction at forward rapidity in ultra-peripheral Pb-Pb collisions at  $\sqrt{s_{NN}} = 5.02$  TeV. *Phys. Lett. B* **2019**, *798*, 134926. [CrossRef]
- [92] Acharya, S. et al. [ALICE Collaboration] Coherent  $J/\psi$  and  $\psi'$  photoproduction at midrapidity in ultra-peripheral Pb-Pb collisions at  $\sqrt{s_{NN}} = 5.02$  TeV. *Eur. Phys. J. C* **2021**, *81*, 712. [CrossRef]
- [93] Bursche, A. (on behalf of the LHCb Collaboration). Study of coherent  $J/\psi$  production in lead-lead collisions at  $\sqrt{s_{NN}} = 5$  TeV with the LHCb experiment. *Nucl. Phys. A* **2019**, *982*, 247–250. [CrossRef]
- [94] Luszczak, A.; Schäfer, W. Coherent photoproduction of  $J/\psi$  in nucleus-nucleus collisions in the color dipole approach—An update. *SciPost Phys. Proc.* **2022**, *8*, 109. [CrossRef]
- [95] Henkels, C.; de Oliveira, E.G.; Pasechnik, R.; Trebien, H. Momentum transfer squared dependence of exclusive quarkonia photoproduction in ultraperipheral collisions. *Phys. Rev. D* **2021**, *104*, 054008. [CrossRef]
- [96] Henkels, C.; de Oliveira, E.G.; Pasechnik, R.; Trebien, H. Exclusive photoproduction of excited quarkonia in ultraperipheral collisions. *Phys. Rev. D* **2020**, *102*, 014024. [CrossRef]
- [97] Ducati, M.B.G.; Griep, M.T.; Machado, M.V.T. Diffractive photoproduction of radially excited  $\psi(2S)$  mesons in photon-Pomeron reactions in PbPb collisions at the CERN Large Hadron Collider. *Phys. Rev. C* **2013**, *88*, 014910. [CrossRef]
- [98] Kopeliovich, B.; Schäfer, A.; Tarasov, A. Nonperturbative effects in gluon radiation and photoproduction of quark pairs. *Phys. Rev. D* **2000**, *62*, 054022. [CrossRef]
- [99] Kopeliovich, B.Z.; Krelina, M.; Nemchik, J.; Potashnikova, I.K. Ultraperipheral nuclear collisions as a source of heavy quarkonia. *Phys. Rev. D* **2023**, *107*, 054005. [CrossRef]
- [100] Acharya, S. et al. [ALICE collaboration] Coherent photoproduction of  $\rho^0$  vector mesons in ultra-peripheral Pb-Pb collisions at  $\sqrt{s_{NN}} = 5.02$  TeV. *J. High Energy Phys.* **2020**, *2020*, 35. [CrossRef]
- [101] Acharya, S. et al. [ALICE Collaboration] First measurement of coherent  $\rho^0$  photoproduction in ultra-peripheral Xe-Xe collisions at  $\sqrt{s_{NN}} = 5.44$  TeV. *Phys. Lett. B* **2021**, *820*, 136481. [CrossRef]
- [102] Baltz, A.J.; Klein, S.R.; Nystrand, J. Coherent vector-meson photoproduction with nuclear breakup in relativistic heavy-ion collisions. *Phys. Rev. Lett.* **2002**, *89*, 012301. [CrossRef]
- [103] Broz, M.; Contreras, J.G.; Tapia Takaki, J.D. A generator of forward neutrons for ultra-peripheral collisions:  $\mathbf{n}_0\mathbf{n}$ . *Comput. Phys. Commun.* **2020**, *253*, 107181. [CrossRef]
- [104] Kryshen, E.; Strikman, M.; Zhalov, M. Photoproduction of  $J/\psi$  with neutron tagging in ultraperipheral collisions of nuclei at RHIC and at the LHC. *Phys. Rev. C* **2023**, *108*, 024904. [CrossRef]

- [105] Acharya, S. et al. [ALICE Collaboration] Energy dependence of coherent photonuclear production of  $J/\psi$  mesons in ultra-peripheral Pb–Pb collisions at  $\sqrt{s_{NN}} = 5.02$  TeV. *J. High Energ. Phys.* **2023**, 2023, 119. [CrossRef]
- [106] Abdulhamid, M.I. et al. [STAR Collaboration] Exclusive  $J/\psi$ ,  $\psi(2s)$ , and  $e^+e^-$  pair production in Au+Au ultraperipheral collisions at BNL Relativistic Heavy Ion Collider. *Phys. Rev. C* **2024**, 110, 014911. [CrossRef]